crystals

MDPI

Article

Synthesis and Structure of Fluorinated (Benzo[*d*]imidazol-2-yl)methanols: Bench Compounds for Diverse Applications

Vasily Romanov [1,2], Evgeny Tretyakov [1,*], Galina Selivanova [1], Jiayao Li [1,2], Irina Bagryanskaya [1], Alexander Makarov [1] and Dominique Luneau [3,*]

1 N. N. Vorozhtsov Novosibirsk Institute of Organic Chemistry, 9 Ac. Lavrentiev Avenue, Novosibirsk 630090, Russia; romanov@nioch.nsc.ru (V.R.); galseliv@nioch.nsc.ru (G.S.); 1455474790ss@gmail.com (J.L.); bagryan@nioch.nsc.ru (I.B.); makarov@nioch.nsc.ru (A.M.)
2 Department of Natural Sciences, Novosibirsk State University, 2 Pirogova Str., Novosibirsk 630090, Russia
3 Campus de La Doua, Université Claude Bernard Lyon-1, 69622 Villeurbanne CEDEX, France
* Correspondence: tretyakov@nioch.nsc.ru (E.T.); dominique.luneau@univ-lyon1.fr (D.L.); Tel.: +7-383-330-9171 (E.T.); +33-472-43-1418 (D.L.)

Received: 5 August 2020; Accepted: 3 September 2020; Published: 4 September 2020



Abstract: A simple and general approach to the synthesis (from commercial precursors) of eight out of nine possible (benzo[*d*]imidazol-2-yl)methanols fluorinated on the benzene ring is reported. Molecular and crystalline structures of most compounds were solved by X-ray diffraction analysis. This made it possible to reveal the influence of the number and arrangement of fluorine atoms in the benzene cycle on the formation of intermolecular hydrogen bonds. It was found that the more fluorine atoms are present in a compound, the higher the dimensionality of the H-bonded structure is. Moreover, the presence of fluorine atoms in the synthesized compounds leads to the emergence of C–F ... π interactions affecting crystal packing. The synthesized fluorinated (benzo[*d*]imidazol-2-yl)methanols may serve as excellent bench compounds for the synthesis of a systematic series of fluorine-containing derivatives to study structure–property correlations in various fields of research from medicine to materials science.

Keywords: polyfluorinated 1,2-diaminobenzenes; heterocyclization; fluorinated benzimidazoles; crystal structure; H-bonding; 1D, 2D, and 3D structures

1. Introduction

Benzimidazoles (1*H*-benzimidazole, 1*H*-benzo[*d*]-imidazole, or 1,3-benzodiazole) occupy an important place in the realm of medicinal chemistry and materials science [1–4]. In nature, the most prominent benzimidazole compound is *N*-ribosyldimethylbenzimidazole, serving as an axial ligand for cobalt in vitamin B_{12} [5]. Benzimidazole derivatives are structural isosteres of naturally occurring nucleotides [6], and this property allows them to interact easily with biopolymers of a living system. This motivates medicinal chemists across the world to synthesize a variety of benzimidazole derivatives and to screen them for various biological activities. Thorough optimization of benzimidazole-based structures has resulted in a large series of various marketed drugs. A far-from-complete list of benzimidazole-based drugs includes antitumor agents (bendamustine and pracinostat), proton pump inhibitors (pantoprazole, lansoprazole, and omeprazole), antiparasitic (albendazole and mebendazole) and antibacterial drugs (ridinilazole), and antihistamine (astemizole and bilastine), antiviral (enviradine, dibazol, and maribavir), and antihypertensive drugs (candesartan, telmisartan, azilsartan, and mibefradil) [7–13]. In addition, benzimidazole-containing pesticides and fungicides (carbendazim,

benomyl, and thiabendazole) have low toxicity at low doses and have been widely used to combat destructive plant pathogens [14–16].

Benzimidazole derivatives are employed as organic catalysts; as ligands for palladium- and rhodium-catalyzed Heck, Suzuki, and reduction reactions and as chiral inductors in asymmetric synthesis [17,18]. They are also applied to the design of highly efficient organic light-emitting devices (OLEDs) [19], water-soluble dyes suitable for electrophotographic deposition [1], and fluorescent materials for medicine, environmental sciences, and chemical engineering [20]. They can also serve as inhibitors of corrosion of metals [21], as electrolytes for fuel cells [22], protective coatings for aerospace applications and fire services [23,24], and as extractants from aqueous media for uranium, thorium, and palladium [25].

Last but not least, benzimidazole-substituted organic paramagnets are actively used as spin carriers in the design of molecular magnets. A large body of work describes magnetostructural studies on benzimidazole-bearing stable nitroxides that are assembled crystallographically by benzimidazole hydrogen bonding. Here, the hydrogen bonds (H-bonds) play a crucial role by acting as crystallographic scaffolding and by assembling radical spin moments into lattices for intermolecular exchanges [26–31]. Benzimidazole-substituted nitronyl nitroxides also hold promise for designing extended exchange-coupled metal-radical networks as illustrated with one-dimensional (1D) and 2D manganese(II) compounds featuring magnetlike behavior with relatively high Curie temperatures (up to 50 K) in the case of the 2D systems [32–38]. Lanthanide complexes with chelating benzimidazole-substituted nitronyl nitroxides have proved to behave as single-molecule magnets, and the radical substituent plays a crucial role in adjusting magnetic relaxation [37,39]. Moreover, some of the complexes possess luminescence correlating with the sign of the lanthanide–radical exchange interaction ($-4.05 < J < 6.1$ K); this phenomenon shows promise for the development of novel multifunctional materials with magneto-optical properties [36].

This huge range of practical applications of benzimidazole is based on a sufficiently small number of starting compounds, and these are mainly 2-substituted or 1,2-disubstituted benzimidazole derivatives. (Benzo[*d*]imidazol-2-yl)methanols and their derivatives are undoubtedly among the basic starting precursors from which numerous functionalized benzimidazoles have been synthesized and then investigated. Practically significant materials prepared from (benzo[d]imidazol-2-yl)methanols include, for example, Co(II) cubane complexes behaving as single-molecule magnets with $T_B > 2$ K (barriers U_{eff}/k_B 21–27 K and relaxation times $\tau_0 = 1.3 \times 10^{-9}$ and 9.7×10^{-9} s) [40], a cobalt catalyst for water electro-oxidation at neutral pH (overpotential 390 mV and a turnover frequency 1.83 s^{-1}) [41], red-emitting fluorophores (quantum yields ~0.96 and near-infrared dyes with absorption maxima near 950 nm [42], cytotoxic and apoptosis-inducing agents [43], and prominent derivatives with antimicrobial activity [44]. As one can see, (benzo[*d*]imidazol-2-yl)methanol itself and its derivatives are used in a wide variety of fields, and they are still key scaffolds in diverse studies and promising projects [45–51].

On the one hand, (benzo[*d*]imidazol-2-yl)methanols have gained so much attention as convenient and affordable starting compounds for the synthesis of substances with useful properties, and on the other hand, fluoro-organic derivatives play an exceptional role in the development of new drugs and the creation of materials with desired qualities [52]. Therefore, we decided to develop and describe in detail the methods for the synthesis of eight out of nine possible fluorinated (benzo[*d*]imidazol-2-yl)methanols (Figure 1a–i). We believe that the availability of different fluorinated and polyfluorinated (benzo[*d*]imidazol-2-yl)methanols as well as their precursors (fluorinated nitroanilines and *o*-phenylenediamines) will be helpful for researchers in various fields because it will allow investigators to obtain a comprehensive series of different fluorine-containing derivatives according to the general schemes.

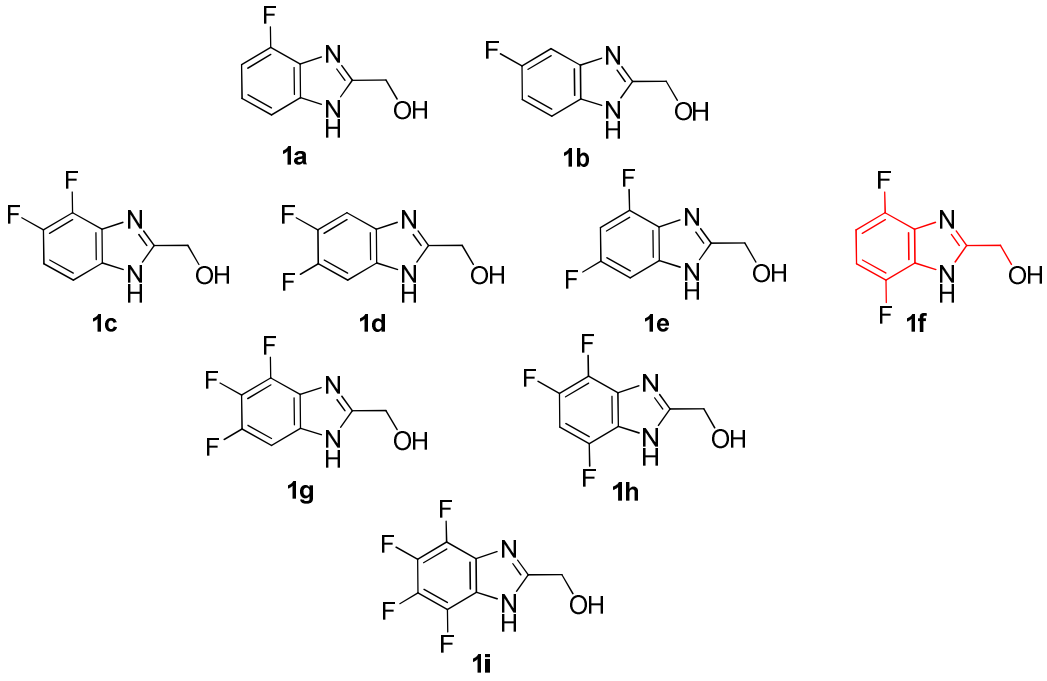


Figure 1. Synthesized in this work (black) and still challenging (red) (benzo[d]imidazol-2-yl)methanols fluorinated on the benzene ring, **1a**–**1i**.

In addition, we showed that according to X-ray diffraction analysis, the number and arrangement of fluorine atoms in (benzo[*d*]imidazol-2-yl)methanols sufficiently influence on their crystal packing. It was found that the more fluorine atoms are present in a compound, the higher the dimensionality of the H-bonded structure is. Moreover, the presence of fluorine atoms in the synthesized compounds leads to the emergence of C–F ... π interactions affecting the crystal packing.

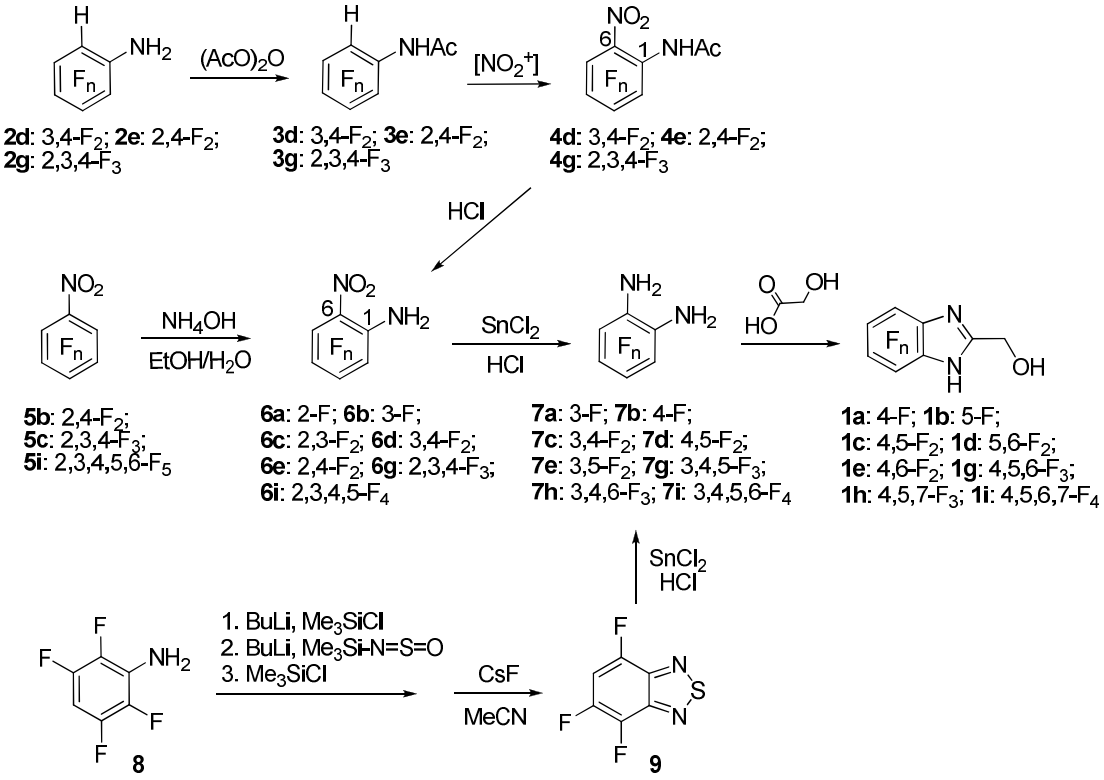
2. Results and Discussion

The chemical transformations leading to the target fluorinated and polyfluorinated (benzo[*d*]imidazol-2-yl)methanols are shown in Scheme 1. Commercially available fluorinated anilines **2d**,**e**,**g** and nitrobenzenes **5b**,**c**,**i** were used as starting substrates. Anilines **2d**,**e**,**g** were acylated to obtain corresponding acetanilides **3**, which were then nitrated by means of a mixture of HNO_3 (70%) with conc. H_2SO_4 (1:1) to prepare nitroacetanilides **4d**,**e**,**g**. Boiling of these nitroacetamides in conc. HCl led to nitroanilines **6d**,**e**,**g** with good yields (80–90%). The range of the nitroanilines thus obtained was expanded via the aminodefluorination reaction of fluorinated nitrobenzenes **5b**,**c**,**i** with aqueous ammonia in EtOH. The reaction gave rise to nitro anilines **6b**,**c**,**i**, which, just as **6d**,**e**,**g** and commercially available **6a**, were reduced to corresponding *o*-phenylenediamines **7a**–**e**,**g**,**i** by the action of $SnCl_2$ in HCl.

A special synthetic route was employed to prepare trifluoro-*o*-phenylenediamine **7h**; the route is based on a reduction in corresponding 4,5,7-trifluoro-2,1,3-benzothiadiazole **9**, which was synthesized by transformation of tetrafluoroaniline **8** into corresponding Ar–N=S=NSiMe$_3$ with its subsequent fluoride-induced nucleophilic ortho-cyclization [53]. Finally, the interaction of fluorinated *o*-phenylenediamines **7a**–**e** and **7g**–**i** with glycolic acid in hydrochloric acid led to target benzo[*d*]imidazol-2-yl)methanols **1a**–**e**,**g**–**i** with good yields (70–85%). All fluorinated benzimidazoles **1** as well as their precursors were fully characterized by spectral methods (Experimental section and Supplementary Materials).

As for difluorobenzimidazole **1f**, within the framework of this work, we failed to design a route for its preparation. The only thing we can say is that this route cannot be based on the use of known 6-nitro-2,5-difluoroaniline or 1,4-difluoro-2,3-dinitrobenzene because these compounds form

only in trace amounts during the nitration of 2,5-difluoroacetanilide or 1,4-difluoro-2-nitrobenzene, respectively [54,55].



Scheme 1. Synthesis of fluorinated (benzo[*d*]imidazol-2-yl)methanols **1a**–**e** and **1g**–**i**.

Well-shaped crystals of compounds **1b**–**e**, **1g**, and **1i** were obtained upon crystallization from acetonitrile or a mixture of acetonitrile with toluene. As to compound **1h**, upon crystallization from various mixtures of solvents, it gave strongly supersaturated solutions with subsequent avalanche-like formation of fine-needle crystals in the form of intergrown hedgehogs.

Molecular and crystal structures of benzimidazoles **1b**–**e**, **1g**, and **1i** were solved by single-crystal X-ray diffraction. The X-ray crystallographic analyses revealed that **1b** and **1e** crystallize in triclinic P–1 space groups, **1c** and **1g** both crystallize in the monoclinic C2/c space group, whereas **1d** in the $P2_1/c$ space group, and **1i** in the tetragonal $P4_12_12$ space group. ORTEP diagrams of dimer H-bonded structures drawn with 50% ellipsoid probability and numbering schemes for these compounds are depicted in Figure 2 below. The diagrams confirm the expected substitution patterns for the synthesized fluorinated benzimidazole series.

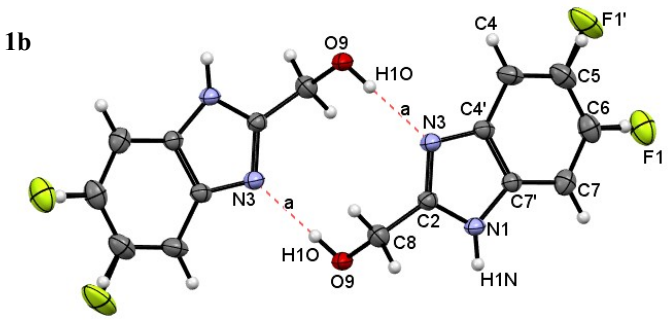


Figure 2. *Cont.*

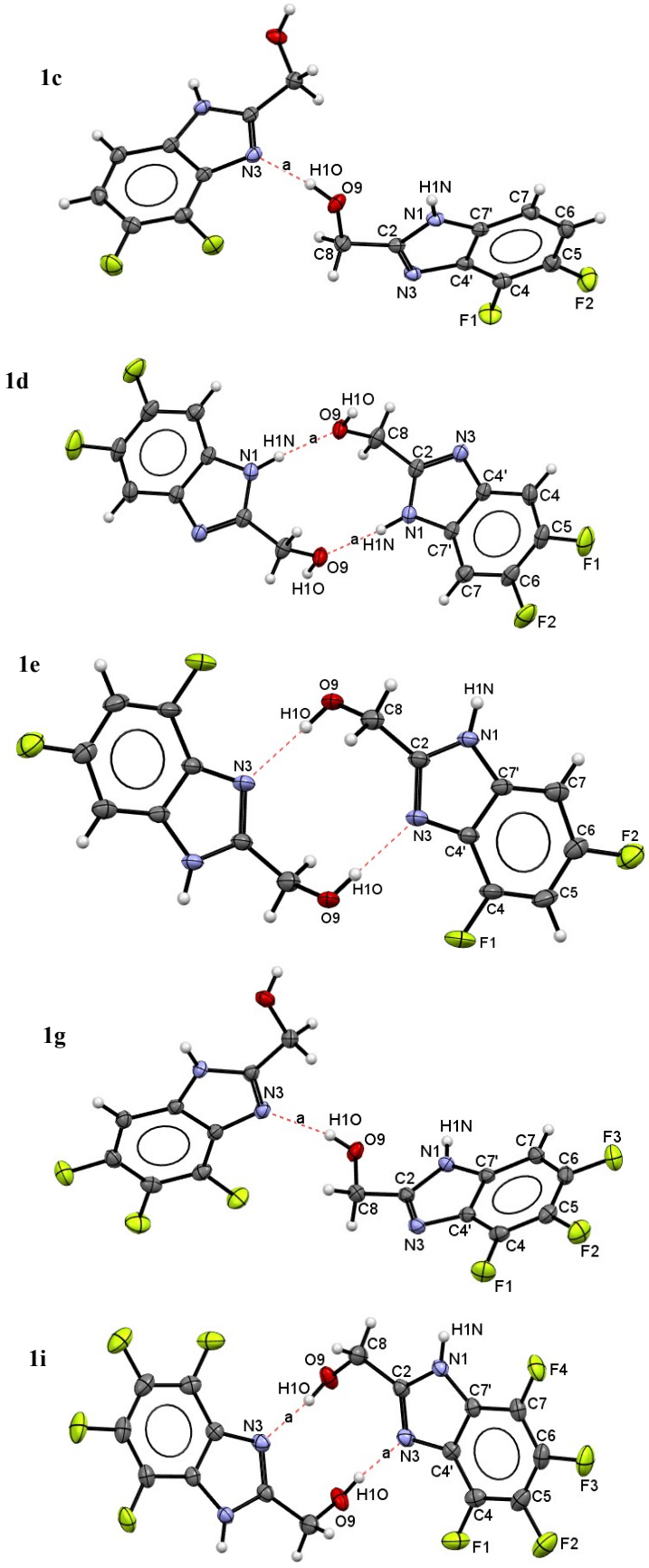


Figure 2. Fragments of crystal structure showing H-bonded dimers of benzimidazoles **1b–e**, **1g**, and **1i**. H-bonds N1–H … O9 and O9–H … N3 are indicated by red dashed lines.

In the investigated benzimidazoles, aromatic nuclei are perfectly planar, and the bond lengths and bond angles are very close to or the same as statistical means [56]. Torsion angles between the aromatic cycle and hydroxymethyl group are in the broad range from 8.12° to 84.45°. These conformation differences are due to dissimilarities in the binding of the molecules through intermolecular H-bonds N–H … O, O–H … N, and C–H … F (Table 1).

To visualize how molecules **1b**–**e**, **1g**, and **1i** are assembled into corresponding crystal structures through H-bonds and short intermolecular contacts, it is reasonable first to choose low-dimensional substructures, for example dimers presented in Figure 2, and then to perform their supramolecular assembly. In **1b**, the propagation of dimers {**1b** … **1b**} via a pair of intermolecular H-bonds N1–H … O9 generates parallel chains running along the [100] direction (Figure 3a). As illustrated in Figure 3b, the final structure is formed due to the binding of chains via H-bonds of type C8–H … F1′ and π–π interactions giving rise to short intermolecular contacts C7′ … C7′ (3.384 Å). Difluorobenzimidazole **1e** is isostructural to monofluoro-derivative **1b**; in its solid state, dimers {**1e** … **1e**} are linked into chains via H-bonds of two types: N1–H … O9 and C8–H … F2 (Supplementary Materials). The latter set the orientation of molecules **1e** in the chains and prevent the disordering observed in compound **1b**. The final supramolecular assembly of chains, as in **1b**, is realized via intermolecular H-bonds C8–H … F1′ and π–π interactions (Supplementary Materials).

In **1c**, **1d**, and **1g** containing two or three adjacent fluorine atoms on the benzene ring, the binding of dimeric synthons via N–H … O and O–H … N hydrogen bonds causes the formation of layers. The compounds **1c** and **1g** are highly isostructural; they both contain a fluorine atom at position 4, also participating in the crosslinking of molecules into layers (Figure 4a). Then, the layers are combined similarly through intermolecular C_{CH_2}–H … F hydrogen bonding and π–π stacking interactions into the final structure (Figure 4b and Supplementary Materials). As for compound **1d**, in its crystals, the supramolecular self-organization of layers is implemented through interlayer short contacts between atoms F2 and C5 (Figure 5).

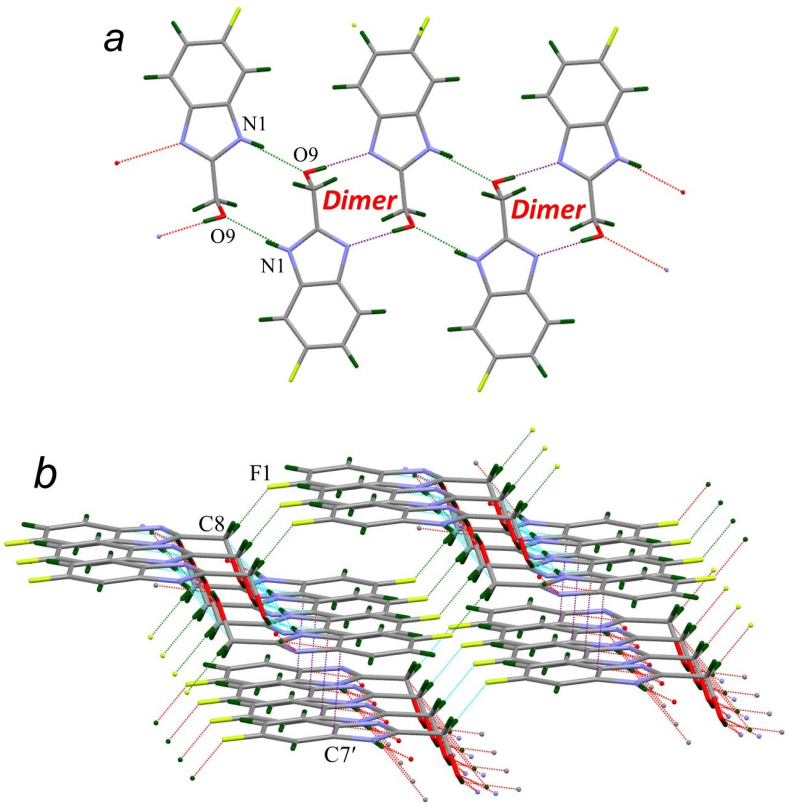


Figure 3. H-bonded chains in the structure of **1b** (**a**) and the binding of the chains via C–H … F and π–π interactions (**b**).

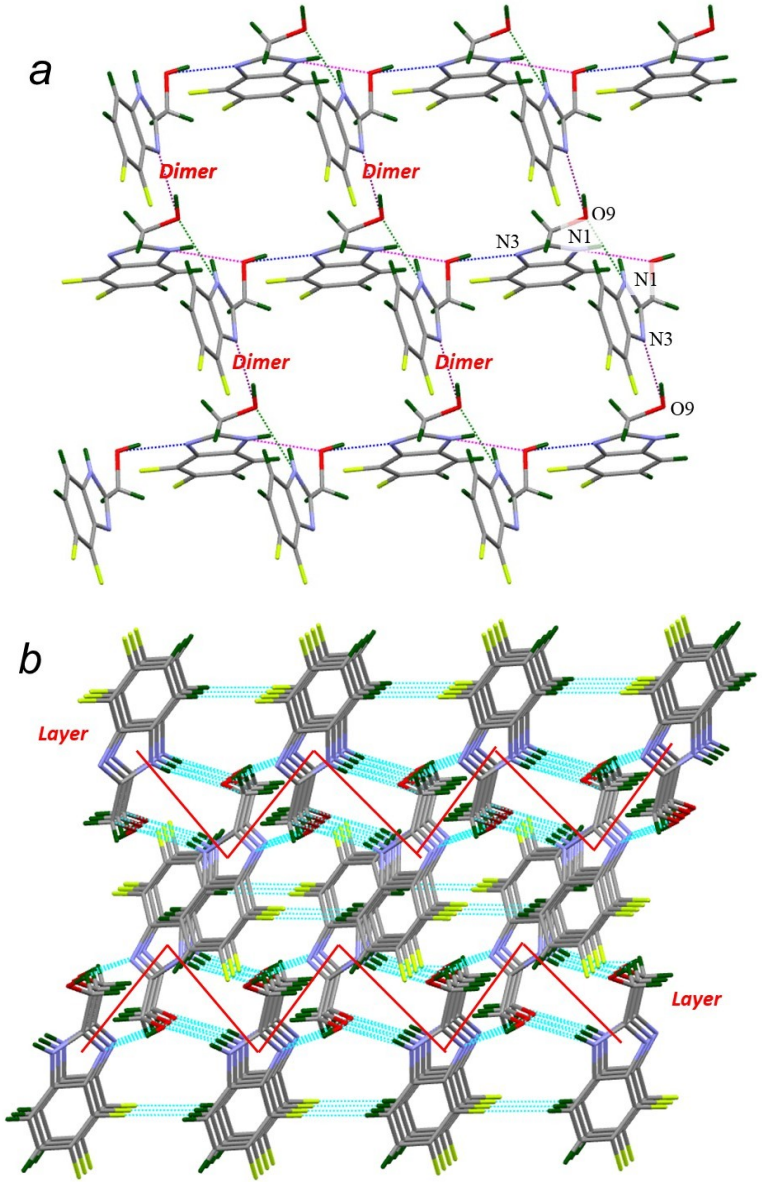


Figure 4. The H-bonded layer in the structure of **1c** (**a**) and assembling of the layers via C_{CH_2}–H . . . F and π–π interactions (**b**).

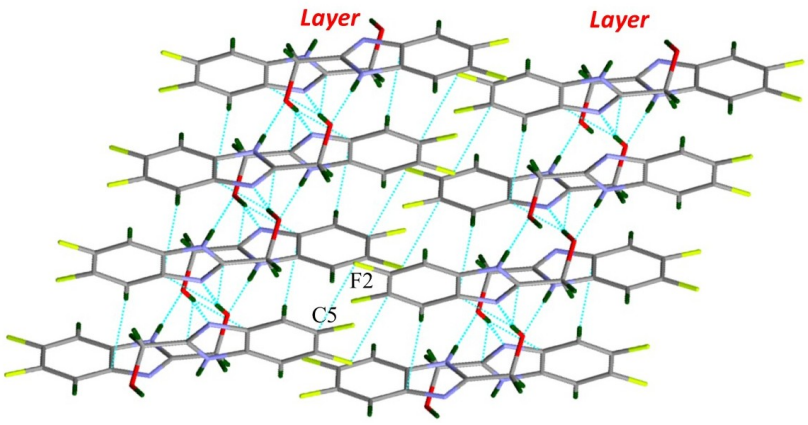


Figure 5. Assembling of layers via C5 . . . F2 interactions in the structure of **1d**.

A further increase in the number of fluorine atoms on the benzene ring gives rise to additional intermolecular interactions, and the tetrafluoro-derivative prefers to bind into a framework (Figure 6). Thus, it is noteworthy that the compounds containing one fluorine atom or not containing neighboring fluorine atoms (**1b** and **1e**) form hydrogen-bonded chains. Compounds **1c**, **1d**, and **1g**, in which benzimidazoles bear two or three adjacent fluorine atoms, form a layered polymeric structure in the solid phase, whereas tetrafluoro-derivative **1i** upon crystallization yields a framework.

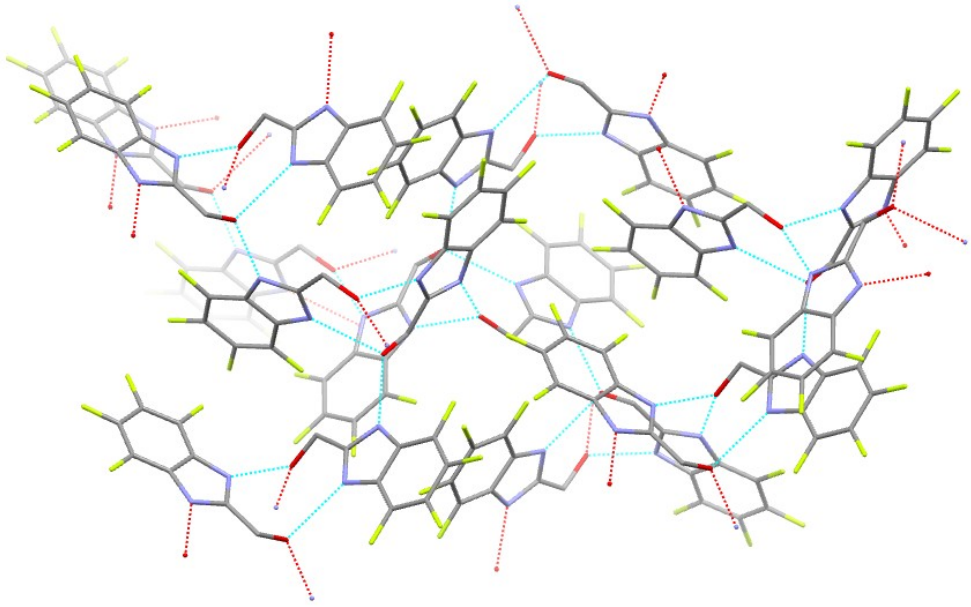


Figure 6. Fragments of the hydrogen-bonded framework in the crystal of compound **1i**.

Table 1. Geometric parameters of H-bonds for **1b**–**e**, **1g**, and **1i**.

Compound	H-Bond	D–H, Å	H … A, Å	D … A, Å	D–H … A, °
1b	N1–H … O9	0.87(3)	1.91(3)	2.766(3)	170(2)
	O9–H … N3	0.82(4)	1.90(4)	2.717(3)	172(3)
	C8–H … F1′	0.97	2.43	3.238(6)	141
1c	N1–H … O9	0.88(2)	2.03(2)	2.849(2)	155(2)
	O9–H … N3	0.88(2)	1.90(2)	2.762(2)	165(2)
	C7–H … F1	0.93	2.53	3.439(2)	166
1d	N1–H … O9	0.89(2)	1.86(2)	2.752(2)	175(2)
	O9–H … N3	0.92(4)	1.80(2)	2.705(2)	172(2)
1e	N1–H … O9	0.91(3)	1.91(3)	2.801(3)	166(2)
	O9–H … N3	0.83(4)	1.95(4)	2.768(3)	168(4)
	C7–H … F1	0.93	2.42	3.242(4)	148
	C8–H … F2	0.97	2.54	3.477(4)	162
1g	N1–H … O9	0.87(2)	2.04(2)	2.828(2)	150(2)
	O9–H … N3	0.81(2)	1.99(2)	2.781(2)	165(2)
	C8–H … F3	0.97	2.44	3.241(2)	139
1i	N1–H … O9	0.85(3)	1.92(3)	2.753(3)	165(2)
	O9–H … N3	0.85(3)	1.89(3)	2.728(2)	172(4)
	C8–H … F1	0.97	2.54	3.180(3)	124

In addition to the preceding discussion of how fluorinated (benzo[*d*]imidazol-2-yl)methanols are bound through H-bonds, their forced mutual orientation is also of interest. Benzimidazole moieties of neighboring molecules are arranged into slipped-parallel stacks with head-to-tail or head-to-head orientations. The distances between planes of aromatic rings are in the range 3.25 to 3.60 Å, and the

intercentroid distances (Cg ... Cg) are 3.44 to 3.98 Å; both are characteristic of π–stacking interactions (Figure 7a). In addition to the π–π interactions, nonvalent contacts between the F atoms and π-systems of neighboring molecules (C–F ... π interactions, Figure 7b) are present in all the compounds except for **1d** in which H ... π interactions take place. Atom-to-plane distances F ... Cg and H ... Cg are 3.25–3.89 and 2.70–2.97 Å, respectively. The energy of these interactions is an order of magnitude or more inferior to the energy of classic H-bonds [57,58]; however, the finding that they take place suggests that they also affect the packing of the fluorinated (benzo[d]imidazol-2-yl)methanols. This observation is worth noting because it indicates that interactions of the C–F ... π type are capable of exerting some influence even on such structures rigidly cross-linked by H-bonds.

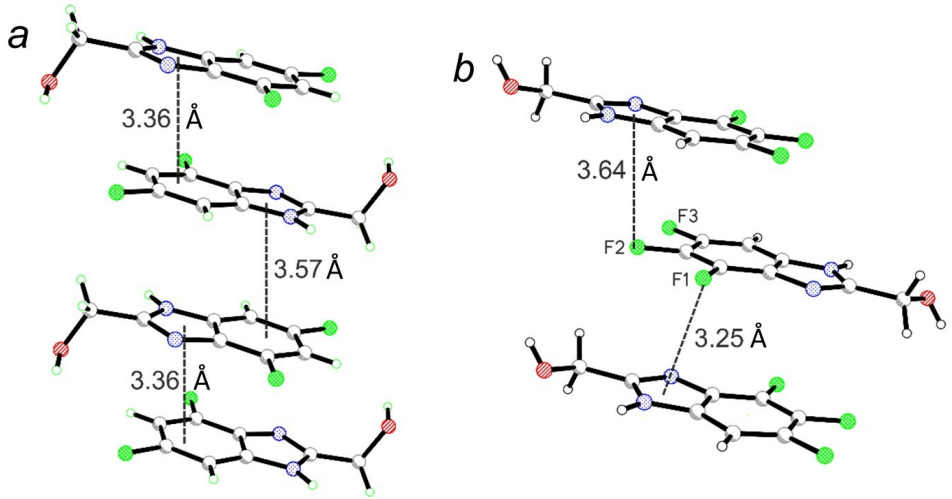


Figure 7. Fragments of crystal structures of **1e** (**a**) and **1g** (**b**) exemplifying π–π stacking and C–F ... π interactions, respectively.

3. Conclusions

In organic chemistry and interdisciplinary research, the identification of correlations between the structure and properties of compounds is of great importance. Given that fluoro-organic derivatives play an important role in the development of new drugs and in the creation of materials with unique properties, basic fluorinated derivatives including heterocyclic compounds are in high demand. The fluorinated (benzo[*d*]imidazol-2-yl)methanols and their key precursors described in this paper can serve as compounds at the bench that will help to obtain a wide variety of products in the fields of medicinal chemistry and materials science. In particular, in our further studies, the synthesized compounds will be utilized for the preparation of benzimidazolyl-substituted nitronyl nitroxide radicals and magnetically active 2D complexes of Mn(II) with these radicals. We hope that a comparative study of magnetic properties of these manganese–nitroxide complexes will enable us to find a way to increase the temperature of transition of the complexes into a magnetically ordered state and will be valuable for further research on the cooperative valence tautomerism phenomenon [32,33,59].

In addition to the synthetic potential of the obtained series of fluorinated (benzo[*d*]imidazol-2-yl)methanols, interesting results were obtained in their X-ray structural analysis. It turned out that weak H-bonds C–H ... F can actively intervene into the interaction of such strong donors and acceptors of H-bonds as the imidazole moiety and hydroxyl group, thus radically changing the nature of the binding of molecules and causing an increase in the resulting structures' dimensionality. Moreover, the presence of fluorine atoms in the synthesized compounds leads to the emergence of other competing and concerted weak intermolecular interactions, like C–F ... π [58,60,61], which to some extent affect the crystal packing too. It is obvious that such interactions can also exist in crystals of derivatives of the synthesized benzimidazoles and thereby affect their properties. Furthermore, it is expected that

such derivatives carrying different fluorinated benzimidazole moieties will interact differently with biological molecules and biological targets.

4. Experimental Section

4.1. General Methods

All solvents were purified by standard procedures. Chemicals were obtained from commercial sources (Merck KGaA, Darmstadt, Germany) and were used without further purification. ^{1}H, ^{13}C, and ^{19}F NMR spectra were recorded on Bruker spectrometers (Bruker Corporation, Billerica, Massachusetts, USA) Avance-300 (300.13, 282.37, and 75.47 MHz for ^{1}H, ^{19}F, and ^{13}C, respectively), Avance-400 (400.13 and 100.61 MHz for ^{1}H and ^{13}C, respectively), DRX-500 and Avance III 500 (500.13 MHz for ^{1}H and 125.76 MHz for ^{13}C), and Avance-600 (151 MHz for ^{13}C). Deuterochloroform ($CDCl_3$), acetone-d_6, and dimethylsulfoxide-d_6 served as solvents, with residual $CHCl_3$ (δ_H = 7.26) or $CDCl_3$ (δ_C = 77.16 ppm), residual acetone (δ_H = 2.05 ppm) or acetone-d_6 (δ_C = 29.8 and 206.3 ppm), and residual dimethylsulfoxide (δ_H = 2.50 ppm) or dimethylsulfoxide-d_6 (δ_C = 39.5 ppm) being internal standards. For ^{19}F spectra, C_6F_6 (δ ^{19}F = −162.9 ppm with respect to $CFCl_3$) was used as an external reference. ^{13}C NMR spectra were registered with C–H spin decoupling. Masses of molecular ions were determined by high-resolution mass spectrometry (HRMS) on a DFS Thermo Scientific instrument at an ionization energy of 70 eV (Thermo Fisher Scientific, Waltham, MA, USA) and by means of Agilent 7200 Accurate Mass Q-TOF GC/MS at an ionization energy of 70 eV (Agilent, Santa Clara, CA, USA). Melting points were registered on a Mettler-Toledo FP900 Thermosystem apparatus (Mettler-Toledo, Greifensee, Switzerland). IR spectra were recorded on a Bruker Vector-22 spectrometer for samples pelleted with KBr (0.25%). UV/Vis spectra were acquired by means of a Cary 5000 instrument (Agilent).

4.2. Interaction of o-Phenylenediamines with Glycolic Acid: The General Procedure

Each *o*-phenylenediamine **7a**–**e** or **7g**–**i** (10.0 mmol) was added to an aqueous 4N HCl solution (20 mL) containing glycolic acid (10.0 mmol). Then, the reaction mixture was refluxed for 8 h, cooled to 0 °C, and alkalized with a ~40% NaOH aqueous solution up to pH ≈ 8. The precipitate was filtered off and washed with ice-cold water to obtain corresponding (benzo[*d*]imidazol-2-yl)methanols **1a**–**e** and **1g**–**i** [62].

4.2.1. (4-Fluorobenzo[*d*]imidazol-2-yl)methanol (**1a**)

Light brown solid; yield 0.23 g (83%), m.p.: 185–186 °C (decomp). IR (KBr), ν/cm^{-1}: 507, 580, 590, 640, 659, 705, 782, 833, 977, 1012, 1052, 1066, 1099, 1141, 1187, 1220, 1267, 1305, 1367, 1421, 1442, 1531, 1552, 1621, 1660, 27442, 2811, 2850, 3099, 3166. UV (EtOH), λ_{max}/nm (lg ε): 204 (4.10), 243 (3.30). ^{1}H NMR (300 MHz, DMSO-d_6), *J*/Hz: δ = 4.68 (s, 2 H, H^{2a}), 6.91 (ddd, *J* = 11.1, *J* = 8.0, *J* = 0.6, 1 H, H^{5}), 7.10 (dt, *J* = 4.9, 2*J* = 8.0, 1 H, H^{6}), 7.29 (d, *J* = 7.9, 1 H, H^{7}).^{19}F NMR (282 MHz, DMSO-d_6, C_6F_6), *J*/Hz: δ = 35.08 (dd, *J* = 11.1, *J* = 4.9, 1 F, F^{4}). ^{13}C NMR (126 MHz, DMSO-d_6), *J*/Hz: δ = 57.60 (s, C^{2a}), 106.4 (d, *J* = 17.3, C^{5}), 108.9 (s, C^{7}), 121.9 (d, *J* = 7.1, C^{6}), 130.1 (d, *J* = 16.1, C^{3a}), 139.1 (s, C^{7a}), 152.3 (d, *J* = 248, C^{4}), 156.2 (s, C^{2}). HRMS (ESI-TOF) calcd. for $C_8H_7FN_2O$ [M]$^{+}$: 166.0537, found: 166.0536.

4.2.2. (5-Fluorobenzo[*d*]imidazol-2-yl)methanol (**1b**)

Cream solid; yield 1.42 g (86%); m.p.: 182–183 °C [44]. IR (KBr), ν/cm^{-1}: 806, 829, 858, 954, 1041, 1108, 1139, 1214, 1249, 1307, 1349, 1446, 1490, 1545, 1600, 1633, 2640, 2789, 2933, 3052, 3115. UV (EtOH), λ_{max}/nm (lg ε): 203 (5.46), 244 (4.79), 279 (4.86), 284 (4.81). ^{1}H NMR (300 MHz, DMSO-d_6), *J*/Hz: δ = 4.66 (s, 2 H, H^{2a}), 6.97 (ddd, 1 H, J_{HH} = 2.4, *J* = 8.7, J_{HF} = 9.6, H^{6}), 7.25 (dd, 1 H, J_{HH} = 2.4, J_{HF} = 9.6, H^{4}), 7.46 (dd, 1 H, J_{HH} = 5.0, J_{HF} = 8.7, H^{7}). ^{19}F NMR (282 MHz, DMSO-d_6), *J*/Hz: δ = 42.84 (br. s, 1 F, F^{5}). ^{13}C NMR (126 MHz, DMSO-d_6), *J*/Hz: δ = 57.6 (s, C^{2a}), 100.9 (s, C^{4}), 109.2 (d, *J* = 25.3, C^{6}), 115.3 (s, C^{7}), 135.0 (s, C^{7a}), 139.1 (s, C^{3a}), 156.7 (s, C^{2}), 158.2 (d, *J* = 233.7, C^{5}). HRMS (ESI-TOF) calcd. for $C_8H_7FN_2O$ [M]$^{+}$: 166.0537, found: 166.0537.

4.2.3. (4,5-Difluorobenzo[*d*]imidazol-2-yl)methanol (**1c**)

Cream solid; yield 1.58 g, (62%), m.p.: 215.9 °C (decomp). IR (KBr), ν/cm^{-1}: 756, 789, 1018, 1058, 1078, 1151, 1230, 1269, 1319, 1429, 1462, 1513, 1544, 1610, 2829, 3143. UV (EtOH), λ_{max}/nm (lg ε): 202 (5.05), 244 (4.28), 273 (4.08). ^{1}H NMR (300 MHz, DMSO-d$_6$), *J*/Hz: δ = 4.68 (br. s, 2 H, H^{2a}), 7.16 (m, 1 H, H^6), 7.25 (m, 1 H, H^7). ^{19}F NMR (282 MHz, DMSO-d$_6$), *J*/Hz: δ = 6.98 (dd, 1 F, J_{FF} = 21.6, J_{HF} = 7.1, F^4), 12.34 (br. dd, 1 F, J_{FF} = 21.6, J_{HF} = 11, F^5). ^{13}C NMR (126 MHz, DMSO-d$_6$), *J*/Hz: δ = 57.5 (s, C^{2a}), 108.0 (s, C^7), 110.6 (d, *J* = 21.2, C^6), 131.2 (s, C^{7a}), 134.4 (s, C^{3a}), 143.7 (dd, *J* = 250.4, *J* = 15.5, C^4), 146.0 (dd, *J* = 233.1, *J* = 10.0, C^5), 157.8 (s, C^2). HRMS (ESI-TOF) calcd. for $C_8H_6F_2N_2O$ [M]$^+$: 184.0443, found: 184.0442.

4.2.4. (5,6-Difluorobenzo[*d*]imidazol-2-yl)methanol (**1d**)

Cream solid; yield 1.44 g (78%); m.p.: 197–199 °C (lit. mp: 198–201 °C [49]). IR (KBr), ν/cm^{-1}: 856, 887, 1039, 1134, 1214, 1284, 1348, 1444, 1475, 1542, 1606, 1641, 2806, 3045, 3101. UV (EtOH), λ_{max}/nm (lg ε): 202 (5.27), 243 (4.70), 278 (4.85), 283 (4.86). ^{1}H NMR (300 MHz, acetone-d$_6$), *J*/Hz: δ = 4.84 (s, 2 H, H^{2a}), 7.42 (d, 1 H, *J* = 9.0, H$^{4 \text{ or } 7}$), 7.45 (d, 1 H, *J* = 9.0, H$^{4 \text{ or } 7}$). ^{19}F NMR (282 MHz, acetone-d$_6$), *J*/Hz: δ = 18.12 (d, *J* = 9.0, 1 F, F$^{5 \text{ or } 6}$), 18.14 (d, *J* = 9.0, 1 F, F$^{5 \text{ or } 6}$). ^{13}C NMR (126 MHz, acetone-d$_6$), *J*/Hz: δ = 58.9 (s, C^{2a}), 103.3 (m, C^{4,7}) 135.1 (s, C^{3a,7a}), 148.1 (dd, *J* = 239, *J* = 17, C^{5,6}), 158.0 (s, C^2). HRMS (ESI-TOF), *m*/*z* [M + H]$^+$ calcd for $C_8H_6F_2N_2O$: 185.0521; found: 185.0522.

4.2.5. (4,6-Difluorobenzo[*d*]imidazol-2-yl)methanol (**1e**)

Dark solid; yield 1.14 g (62%); m.p.: 192–193 °C. IR (KBr), ν/cm^{-1}: 835, 862, 982, 1010, 1041, 1085, 1120, 1216, 1249, 1361, 1429, 1444, 1506, 1545, 1606, 1645, 2827, 3120. UV (EtOH), λ_{max}/nm (lg ε): 206 (5.32), 242 (4.72), 267 (4.62), 271 (4.62), 275 (4.63). ^{1}H NMR (300 MHz, DMSO-d$_6$), *J*/Hz: δ = 4.83 (s, 2 H, H^{2a}), 7.27 (td, 1 H, J_{HF} = 10.6, J_{HH} = 2.2, H^5), 7.34 (dd, 1 H, J_{HF} = 8.4, J_{HH} = 2.2, H^7). ^{19}F NMR (282 MHz, DMSO-d$_6$), *J*/Hz: δ = 39.90 (dd 1 F, J_{FH} = 10.6, J_{FF} = 3.5, F^4), 49.69 (br. s, 1 F, F^6). ^{13}C NMR (126 MHz, DMSO-d$_6$), *J*/Hz: δ = 56.1 (s, C^{2a}), 96.4 (dd, *J* = 27.3, *J* = 4.6, C^7), 99.3 (dd, *J* = 29.8, *J* = 21.3, C^5), 121.5 (d, *J* = 16.5, C^{3a}), 135.3 (dd, *J* = 15.6, *J* = 9.0, C^{7a}), 149.8 (dd, *J* = 251.0, *J* = 15.2, C^4), 156.7 (d, *J* = 1.2, C^2), 158.5 (dd, *J* = 240.0, *J* = 10.8, C^6). HRMS (ESI-TOF), *m*/*z* [M]$^+$ calcd for $C_8H_6F_2N_2O$: 184.0443; found: 184.0441.

4.2.6. (4,5,6-Trifluorobenzo[*d*]imidazol-2-yl)methanol (**1g**)

Cream solid; yield 1.58 g (78%); m.p.: 198–201 °C. IR (KBr), ν/cm^{-1}: 823, 852, 962, 1033, 1048, 1081, 1120, 1234, 1253, 1365, 1433, 1448, 1516, 1535, 1616, 1643, 2836, 3153. UV (EtOH), λ_{max}/nm (lg ε): 211 (4.96), 238 (4.61), 273 (4.73), 278 (4.54), 283 (4.33). ^{1}H NMR (300 MHz, DMSO-d$_6$), *J*/Hz: δ = 4.67 (s, 2 H, H^{2a}), 7.35 (ddd, 1 H, J_{HF} = 10.2, J_{HF} = 6.3, J_{HF} = 1.7, H^7), 8.2 (br. s, 1H, NH). ^{19}F NMR (282 MHz, DMSO-d$_6$,), *J*/Hz: δ = −6.94 (br. td, 1 F, 2J_{FF} = 21, J_{HF} = 6.5, F^5), 12.60 (br. d, 1 F, J_{FF} = 21, F^4), 21.34 (dd, 1 F, *J* = 21, *J* = 10.2, F^6). ^{13}C NMR (126 MHz, DMSO-d$_6$), *J*/Hz: δ = 57.6 (s, C^{2a}), 96.1 (dd, *J* = 22.0, *J* = 3.0, C^7), 126.9 (d, *J* = 11.3, C^{3a}), 131.6 (dd, *J* = 13.0, *J* = 9.7, C^{7a}), 134.2 (ddd, *J* = 237.0, *J* = 17.8, *J* = 13.2, C^4), 139.2 (ddd, *J* = 252.0, *J* = 12.0, *J* = 4.9, C^5), 145.6 (dd, *J* = 238.0, *J* = 12.0, C^6), 158.3 (s, C^2). HRMS (ESI-TOF) calcd. for $C_8H_5F_3N_2O$ [M]$^+$: 202.1335, found: 202.1334.

4.2.7. (4,5,7-Trifluorobenzo[*d*]imidazol-2-yl)methanol (**1h**)

Cream solid; yield 0.48 g (96%); m.p.: 196–197 °C (decomp). IR (KBr), ν/cm^{-1}: 507, 580, 590, 640, 659, 705, 782, 833, 977, 1012, 1052, 1066, 1099, 1141, 1187, 1220, 1267, 1305, 1367, 1421, 1442, 1531, 1552, 1621, 1660, 27442, 2811, 2850, 3099, 3166. UV (EtOH), λ_{max}/nm (lg ε): 204 (5.12), 243 (4.13). ^{1}H NMR (300 MHz, DMSO-d$_6$), *J*/Hz: δ = 4.69 (s, 2 H, H^{2a}), 5.81 (br. s, OH), 7.25 (ddd, 1 H, J_{HF} = 12, J_{HF} = 10, J_{HF} = 5.7, H^6). ^{19}F NMR (282 MHz, DMSO-d$_6$, C$_6$F$_6$), *J*/Hz: δ = 5.38 (br. dt, 1 F, 2J_{FF} = ~20, J_{FH} = ~4.3, F^4), 18.45 (br. s, 1 F, F^5). 33.49 (br. dd, 1 F, J_{FF} = ~20.0, J_{FH} = ~10, F^7).^{13}C NMR (126 MHz, DMSO-d$_6$), *J*/Hz: δ = 57.4 (s, C^{2a}), 97.9 (t, 2*J* = 24.5, C^6), 125.2 (br. s, C^{7a}), 129.9 (br. s, C^{3a}), 135.3 (br. d, *J* = 244, C^4),

143.8 (dt, J = 236.2, 2J = 11.6, C^5), 145.1 (br. d, J = 264 C^7), 157.8 (s, C^2). HRMS (ESI-TOF) calcd. for $C_8H_5F_3N_2O$ $[M]^+$: 202,1334, found: 202.1334.

4.2.8. (4,5,6,7-Tetrafluorobenzo[*d*]imidazol-2-yl)methanol (**1i**)

Cream solid; yield 2.11 g (96%); m.p.: 186–187 °C. 777, 785, 1023, 1064, 1078, 1152, 1247, 1264, 1338, 1414, 1465, 1544, 1556, 1623, 2837, 3167. UV (EtOH), λ_{max}/nm (lg ε): 205 (5.12), 234 (4.63), 274 (3.88). 311 (3.45). ^{1}H NMR (300 MHz, DMSO-d_6), J/Hz: δ = 4.67 (s, 2 H, H^{2a}), 5.99 (br. s, 2 H, $H^{NH,OH}$). ^{19}F NMR (282 MHz, DMSO-d_6), J/Hz: δ = −6.68 (m, 2 F, $F^{5,6}$), 5.65 (m, 2 F, $F^{4,7}$). ^{13}C NMR (126 MHz, DMSO-d_6), J/Hz: δ = 57.7 (s, C^{2a}), 125.2 (d, J = 8.6, $C^{3a\ or\ 7a}$), 125.3 (d, J = 9.3, $C^{3a\ or\ 7a}$), 134.4–134.2 (m, $C^{5,6}$), 136.5–136.2 (m, $C^{4,7}$), 159.5 (s, C^2). HRMS (ESI-TOF) calcd. for $C_8H_4F_4N_2O$ $[M]^+$: 220.1239, found: 220.1239.

4.3. Single-Crystal X-ray Diffraction Analyses

These analyses of **1b**–**1e**, **1g**, and **1i** were performed on a Bruker Kappa Apex II CCD diffractometer using φ,ω-scans of narrow (0.5°) frames with Mo Kα radiation (λ = 0.71073 Å) and a graphite monochromator. The structures were solved by direct methods in the SHELX-97 software [63] and were refined by the full-matrix least-squares method against all F2 in anisotropic approximation using SHELXL-2014/7 [64]. Absorption corrections were applied via the empirical multiscan method by means of the SADABS software [65]. The hydrogen atoms' positions, except for H atoms in NH and OH groups, were calculated with the riding model. Nitrogen-bound and oxygen-bound H atoms were located on a difference Fourier map and refined freely. The resultant crystal structures were analyzed for short contacts between nonbonded atoms using PLATON [66,67] and MERCURY [68]. General crystallographic data for these compounds are summarized in Table 2.

CCDC 2016713–2016718 contain the supplementary crystallographic data for benzimidazoles **1b**–**e**, **1g**, and **1i**, respectively. These data can be obtained free of charge via http://www.ccdc.cam.ac.uk/cgi-bin/catreq.cgi or from the Cambridge Crystallographic Data Centre, 12 Union Road, Cambridge CB2 1EZ, UK; Fax: (+44)-1223-336-033 or by e-mail: deposit@ccdc.cam.ac.uk.

Table 2. X-ray diffraction data for compounds **1b**–**e**, **1g**, and **1i**.

Compound	1b	1c	1d
Empirical formula	$C_8H_7F_1N_2O$	$C_8H_6F_2N_2O$	$C_8H_6F_2N_2O$
Formula weight	166.16	184.15	184.15
Temperature, K	296(2)	296(2)	296(2)
Wavelength, Å	0.71073	0.71073	0.71073
Crystal system	Triclinic	Monoclinic	Monoclinic
Space group	P-1	C2/c	$P2_1/c$
Unit cell dimensions *a*, Å	7.139(2)0	12.5909(4)	9.7021(7)
b, Å	7.321(2)	8.4163(4)	12.0410(8)
c, Å	8.362(2)	14.3912(5)	7.3374(5)
α, °	103.15(1)	90	90
β, °	106.17(1)	95.608(2)	109.122(3)
γ, °	102.63(1)	90	90
Volume, Å^3	389.7(2)	1517.7(1)	809.9(1)
Z	2	8	4
Density (calcd.), Mg·m^{-3}	1.416	1.612	1.510
Abs. coefficient, mm^{-1}	0.113	0.143	0.134
F(000)	172	752	376
Crystal size, mm^3	0.03 × 0.20 × 0.70	0.40 × 0.50 × 0.60	0.02 × 0.70 × 0.70
Θ range for data collection, °	2.7–27.7	2.8–29.5	2.2–30.0
Index ranges	−9 ≤ h ≤ 9, −9 ≤ k ≤ 9, −10 ≤ l ≤ 10	−15 ≤ h ≤17, −10 ≤ k ≤ 11, −18 ≤ l ≤18	−13≤ h ≤ 3, −16 ≤ k ≤ 16, −10 ≤ l ≤ 10
Reflections collected	6241	9855	9703
Independent reflections	1790 R(int) = 0.028	1831 R(int) = 0.057	2143 R(int) = 0.038
Completeness to θ, %	99.3	99.3	99.9 (θ ≤ 25°)
Data/restraints/parameters	1790/0/125	1831/0/124	2143/0/124
Goodness-of-fit on F^2	1.02	1.02	1.02
Final R indices $I > 2\sigma(I)$	R_1 = 0.0519, wR_2 = 0.1448	R_1 = 0.0442, wR_2 = 0.1167	R_1 = 0.0423, wR_2 = 0.1037
Final R indices (all data)	R_1 = 0.0672, wR_2 = 0.1564	R_1 = 0.0514, wR_2 = 0.1245	R_1 = 0.0583, wR_2 = 0.1162
Largest diff. peak/hole, e·Å^{-3}	0.20/−0.15	0.22/−0.22	0.19/−0.21
CCDC	2016713	2016714	2016715

Table 2. *Cont.*

Compound	1e	1g	1i
Empirical formula	$C_8H_6F_2N_2O$	$C_8H_5F_3N_2O$	$C_8H_4F_4N_2O$
Formula weight	184.15	202.14	220.13
Temperature, K	296(2)	296(2)	296(2)
Wavelength, Å	0.71073	0.71073	0.71073
Crystal system	Triclinic	Monoclinic	Tetragonal
Space group	P-1	C2/c	$P4_12_12$
Unit cell dimensions *a*, Å	7.2007(8)	12.6623(8)	10.8539(3)
b, Å	7.2524(7)	8.3996(8)	10.8539(3)
c, Å	8.7419(8)	14.770(1)	14.3674(4)
α, °	107.112(3)	90	90
β, °	108.156(3)	92.769(4)	90
γ, °	104.107(3)	90	90
Volume, Å^3	385.27(7)	1569.0(2)	1692.6(1)
Z	2	8	8
Density (calcd.), Mg·m^{-3}	1.587	1.711	1.728
Abs. coefficient, mm^{-1}	0.140	0.164	0.176
F(000)	188	816	880
Crystal size, mm^3	0.08 × 0.15 × 0.25	0.08 × 0.12 × 0.30	0.15 × 0.50 × 0.80
Θ range for data collection, °	2.8–27.5	2.8–27.6	2.4–29.5
Index ranges	$-9 \le h \le 9$, $-9 \le k \le 9$, $-11 \le l \le 10$	$-16 \le h \le 16$, $-10 \le k \le 10$, $-19 \le l \le 19$	$-14 \le h \le 14$, $-14 \le k \le 15$, $-19 \le l \le 17$
Reflections collected	6116	15,950	27,896
Independent reflections	1748 R(int) = 0.028	1804 R(int) = 0.045	2178 R(int) = 0.039
Completeness to θ, %	99.7 (θ ≤ 25°)	99.8	100.0 (θ ≤ 25°)
Data/restraints/parameters	1748/0/124	1804/0/133	2178/0/142
Goodness-of-fit on F^2	1.04	1.00	1.04
Final R indices $I > 2\sigma(I)$	$R_1 = 0.0520$, $wR_2 = 0.1406$	$R_1 = 0.0359$, $wR_2 = 0.0872$	$R_1 = 0.0347$, $wR_2 = 0.0835$
Final R indices (all data)	$R_1 = 0.0849$, $wR_2 = 0.1656$	$R_1 = 0.0458$, $wR_2 = 0.0948$	$R_1 = 0.0462$, $wR_2 = 0.0932$
Largest diff. peak/hole, e·Å^{-3}	0.47, −0.26	0.28, −0.15	0.14, −0.19
CCDC	2016716	2016717	2016718

Supplementary Materials: The following is available online at http://www.mdpi.com/2073-4352/10/9/786/s1. The list of prepared acetanilides **3**; nitroacetanilides **4**, nitroanilines **5** and **6**, and *o*-phenylenediamines **7**; NMR spectra; fragments of crystal structures of **1b**, **1c**, **1d**, **1e**, **1g**, and **1i**.

Author Contributions: Conceptualization, E.T. and D.L.; methodology, V.R. and G.S.; investigation, V.R., G.S., J.L., I.B. and A.M.; writing—original draft preparation, E.T. and D.L.; supervision, E.T. and G.S.; project administration, E.T.; funding acquisition, E.T. and D.L. All authors have read and agreed to the published version of the manuscript.

Funding: This research was funded by the Ministry of Science and Higher Education of the Russian Federation (the Affiliate Program of Hubert Curien–A.N. Kolmogorov, identifier RFMEFI61619 × 0116).

Acknowledgments: The authors would like to acknowledge the Multi-Access Chemical Research Center SB RAS for spectral and analytical measurements.

Conflicts of Interest: The authors declare no conflict of interest.

References

1. Marinescu, M. *Chemistry and Applications of Benzimidazole and Its Derivatives*; IntechOpen: London, UK, 2019.
2. Vestergaard, A.A. *Benzimidazole: Preparation and Applications*; Nova Science Publishers: Hauppauge, NY, USA, 2020.
3. Selivanova, G.A.; Tretyakov, E.V. Fluorinated benzimidazoles for medicinal chemistry and new materials. *Russ. Chem. Bull.* **2020**, *69*, 838–858. [CrossRef]
4. Rajasekhar, S.; Maiti, B.; Balamurali, M.M.; Chanda, K. Synthesis and medicinal applications of benzimidazoles: An overview. *Curr. Org. Synth.* **2017**, *14*, 40–60. [CrossRef]
5. Barker, H.A.; Smyth, R.D.; Weissbach, H.; Toohey, J.I.; Ladd, J.N.; Volcani, B.E. Isolation and properties of crystalline cobamide coenzymes containing benzimidazole or 5,6-dimethylbenzimidazole. *J. Biol. Chem.* **1960**, *235*, 480–488.
6. Arjmand, F.; Mohani, B.; Ahmad, S. Synthesis, antibacterial, antifungal activity and interaction of CT-DNA with a new benzimidazole derived Cu(II) complex. *Eur. J. Med. Chem.* **2005**, *40*, 1103–1110. [CrossRef]
7. Bansal, Y.; Silakari, O. The therapeutic journey of benzimidazoles: A review. *Bioorg. Med. Chem.* **2012**, *20*, 6208–6236. [CrossRef]

8. Moniruzzaman, R.S.; Mahmud, T. Quantum chemical and pharmacokinetic studies of some proton pump inhibitor drugs. *Am. J. Biomed. Sci. Res.* **2019**, *2*, 259–264.
9. Njar, V.C.; Brodie, A.M. Discovery and development of Galeterone (TOK-001 or VN/124-1) for the treatment of all stages of prostate cancer. *J. Med. Chem.* **2015**, *58*, 2077–2087. [CrossRef]
10. Tahlan, S.; Kumar, S.; Ramasamy, K.; Lim, S.M.; Shah, S.A.A.; Mani, V.; Pathania, R.; Narasimhan, B. Design, synthesis and biological profile of heterocyclic benzimidazole analogues as prospective antimicrobial and antiproliferative agents. *BMC Chem.* **2019**, *13*, 50–64. [CrossRef] [PubMed]
11. Scholten, W.K.; Christensen, A.E.; Olesen, A.E.; Drewes, A.M. Quantifying the adequacy of opioid analgesic consumption globally: An updated method and early findings. *Am. J. Public Health* **2019**, *109*, 52–57. [CrossRef]
12. Salahuddin; Shaharyar, M.; Mazumder, A. Benzimidazoles: A biologically active compounds. *Arab. J. Chem.* **2017**, *10*, S157–S173. [CrossRef]
13. Han, X.-F.; He, X.; Wang, M.; Xu, D.; Hao, L.-P.; Liang, A.-H.; Zhang, J.; Zhou, Z.-M. Discovery of novel, potent and low-toxicity angiotensin II receptor type 1 (AT1) blockers: Design, synthesis and biological evaluation of 6-substituted aminocarbonyl benzimidazoles with a chiral center. *Eur. J. Med. Chem.* **2015**, *103*, 473–487. [CrossRef] [PubMed]
14. Wang, X.; Chen, Y.-F.; Yan, W.; Cao, L.-L.; Ye, Y.-H. Synthesis and biological evaluation of benzimidazole phenylhydrazone derivatives as antifungal agents against phytopathogenic fungi. *Molecules* **2016**, *21*, 1574. [CrossRef] [PubMed]
15. Gupta, R.C. Toxicity of Fungicides. In *Veterinary Toxicology*, 3rd ed.; Academic Press: Cambridge, MA, USA, 2018; pp. 569–580.
16. Ermler, S.; Scholze, M.; Kortenkamp, A. Seven benzimidazole pesticides combined at sub-threshold levels induce micronuclei in vitro. *Mutagenesis* **2013**, *28*, 417–426. [CrossRef] [PubMed]
17. Said, N.R.; Mustakim, M.A.; Sani, M.M.M.; Baharin, S.N.A. Heck reaction using palladium-benzimidazole catalyst: Synthesis, characterisation and catalytic activity. *IOP Conf. Ser. Mater. Sci. Eng.* **2018**, *458*, 012019. [CrossRef]
18. Günnaz, S.; Gökçe, A.G.; Türkmen, H. Synthesis of bimetallic complexes bridged by 2,6-bis(benzimidazol-2-yl)pyridine derivatives and their catalytic properties in transfer hydrogenation. *Dalton Trans.* **2018**, *47*, 17317–17328. [CrossRef]
19. Zhao, Y.; Chao, W.; Qiu, P.; Li, X.; Wang, Q.; Chen, J.; Ma, D. New benzimidazole-based bipolar hosts: Highly efficient phosphorescent and thermally activated delayed fluorescent organic light-emitting diodes employing the same device structure. *ACS Appl. Mater. Interfaces* **2016**, *8*, 2635–2643. [CrossRef]
20. Horak, E.; Kassal, P.; Steinberg, M. Benzimidazole as a structural unit in fluorescent chemical sensors: The hidden properties of a multifunctional heterocyclic scaffold. *Supramol. Chem.* **2017**, *30*, 838–857. [CrossRef]
21. Eldebss, T.M.A.; Farag, A.M.; Shamy, A.Y.M. Synthesis of some benzimidazole-based heterocycles and their application as copper corrosion inhibitors. *J. Heterocycl. Chem.* **2019**, *56*, 371–390. [CrossRef]
22. Yuan, S.; Guo, X.; Aili, D.; Pan, C.; Li, Q.; Fang, J. Poly(imide benzimidazole)s for high temperature polymer electrolyte membrane fuel cells. *J. Membr. Sci.* **2014**, *454*, 351–358. [CrossRef]
23. Igbal, H.M.S.; Bhowmik, S.; Benedictus, R. Performance evaluation of polybenzimidazole coating for aerospace application. *Prog. Org. Coat.* **2017**, *105*, 190–199. [CrossRef]
24. Mandal, S.; Song, G. Characterizing thermal protective fabrics of firefighters' clothing in hot surface contact. *J. Ind. Text.* **2016**, *47*, 622–639. [CrossRef]
25. Veeraragavan, V.; Kumar, C.R.; Suresh, A.; Jayalakshmi, S.; Mudali, K.M.; Sivaraman, N. Evaluation of polybenzimidazole-based polymers for the removal of uranium, thorium and palladium from aqueous medium. *R. Soc. Open Sci.* **2018**, *5*, 171701.
26. Lahti, P.M. Structure-property relationships for metal-free organic magnetic materials. *Adv. Phys. Org. Chem.* **2011**, *45*, 93–169.
27. Adriano, C.; Freitas, R.S.; Paduan-Filho, A.; Pagliuso, P.G.; Oliveira, N.F.; Lahti, P.M. Magnetic phase diagram of the organic antiferromagnet F_4BImNN. *Polyhedron* **2017**, *136*, 2–4. [CrossRef]
28. Lescop, C.; Luneau, D.; Bussiere, G.; Triest, M.; Reber, C. Ligand-Centered Near-Infrared Luminescence from Lanthanide Complexes with Chelating Nitronyl Nitroxide Free Radicals. *Inorg. Chem.* **2000**, *39*, 3740–3741. [CrossRef]

29. Seber, G.; Freitas, R.S.; Mague, J.T.; Paduan-Filho, A.; Gratens, X.; Bindilatti, V.; Oliveira, N.F.; Yoshioka, N.; Lahti, P.M. Magnetic tuning of all-organic binary alloys between two stable radicals. *J. Am. Chem. Soc.* **2012**, *134*, 3825–3833. [CrossRef] [PubMed]
30. Sugano, T.; Blundell, S.J.; Lancaster, T.; Pratt, F.L.; Mori, H. Magnetic order in the purely organic quasi-one-dimensional ferromagnet 2-benzimidazolyl nitronyl nitroxide. *Phys. Rev. B* **2010**, *82*, 180401. [CrossRef]
31. Naoki, Y.; Munetoshi, I.; Yuichiro, M.; Takanari, K.; Hidenari, I.; Shigeru, O. Unusually large magnetic interactions observed in hydrogen-bonded nitronyl nitroxides. *Chem. Lett.* **1997**, *26*, 251–252.
32. Luneau, D. Coordination chemistry of nitronyl nitroxide radicals has memory. *Eur. J. Inorg. Chem.* **2020**, *7*, 597–604. [CrossRef]
33. Luneau, D.; Borta, A.; Chumakov, Y.; Jacquot, J.-F.; Jeanneau, E.; Lescop, C.; Rey, P. Molecular magnets based on two-dimensional Mn(II)-nitronyl nitroxide frameworks in layered structures. *Inorg. Chim. Acta* **2008**, *361*, 3669–3676. [CrossRef]
34. Luneau, D.; Rey, P. Magnetism of metal-nitroxide compounds involving bis-chelating imidazole and benzimidazole substituted nitronyl nitroxide free radicals. *Coord. Chem. Rev.* **2005**, *249*, 2591–2611. [CrossRef]
35. Lescop, C.; Bussiere, G.; Beaulac, R.; Belisle, H.; Belorizky, E.; Rey, P.; Reber, C.; Luneau, D. Magnetic and optical properties of nitroxide radicals and their lanthanide complex. *J. Phys. Chem. Solids* **2004**, *65*, 773–779. [CrossRef]
36. Lescop, C.; Luneau, D.; Rey, P.; Bussiere, G.; Reber, C. Synthesis, structures, and magnetic properties of a series of lanthanum(III) and gadolinium(III) complexes with chelating benzimidazole-substituted nitronyl nitroxide free radicals. Evidence for antiferromagnetic Gd(III)-radical interactions. *Inorg. Chem.* **2002**, *41*, 3375–3384. [CrossRef] [PubMed]
37. Fegy, K.; Luneau, D.; Belorizky, E.; Novac, M.; Tholence, J.L.; Paulsen, C.; Ohm, T.; Rey, P. 1D Manganese(II) Derivatives of an Imidazole-Substituted Nitronyl Nitroxide. An Approach toward Molecular Magnetic Materials of High Dimensionality. *Inorg. Chem.* **1998**, *37*, 4524–4532. [CrossRef] [PubMed]
38. Fegy, K.; Luneau, D.; Ohm, T.; Paulsen, C.; Rey, P. Two-dimensional nitroxide-based molecular magnetic materials. *Angew. Chem. Int. Ed.* **1998**, *37*, 1270–1273. [CrossRef]
39. Hu, P.; Zhu, M.; Mei, X.; Tian, H.; Ma, Y.; Li, L.; Liao, D. Single-molecule magnets based on rare earth complexes with chelating benzimidazole-substituted nitronyl nitroxide radicals. *Dalton Trans.* **2012**, *41*, 14651–14656. [CrossRef]
40. Ma, X.-F.; Wang, Z.; Chen, X.-L.; Kurmoo, M.; Zeng, M.-H. Ligand effect on the single-molecule magnetism of tetranuclear Co(II) cubane. *Inorg. Chem.* **2017**, *56*, 15178–15186. [CrossRef]
41. Chen, B.-T.; Morlanes, N.; Adogla, E.; Takanabe, K.; Rodionov, V.O. An efficient and stable hydrophobic molecular cobalt catalyst for water electro-oxidation at neutral pH. *ACS Catal.* **2016**, *6*, 4647–4652. [CrossRef]
42. Patalag, L.J.; Jones, P.G.; Werz, D.B. BOIMPYs: Rapid access to a family of red-emissive fluorophores and NIR dyes. *Angew. Chem. Int. Ed.* **2016**, *55*, 13340–13344. [CrossRef]
43. Sharma, P.; Srinivasa Reddy, T.; Thummuri, D.; Senwar, K.R.; Kumar, N.P.; Naidu, V.G.M.; Bhargava, S.K.; Shankaraiah, N. Synthesis and biological evaluation of new benzimidazole-thiazolidinedione hybrids as potential cytotoxic and apoptosis inducing agents. *Eur. J. Med. Chem.* **2016**, *124*, 608–621. [CrossRef]
44. Alasmary, F.A.S.; Snelling, A.M.; Zain, M.E.; Alafeefy, A.M.; Awaad, A.S.; Karodia, N. Synthesis and evaluation of selected benzimidazole derivatives as potential antimicrobial agents. *Molecules* **2015**, *20*, 15206–15223. [CrossRef] [PubMed]
45. Shang, Y.; Hao, Q.; Jiang, K.; He, M.; Wang, J. Discovery of heterocyclic carbohydrazide derivatives as novel selective fatty acid amide hydrolase inhibitors: Design, synthesis and anti-neuroinflammatory evaluation. *Bioorg. Med. Chem. Lett.* **2020**, *30*, 127118. [CrossRef] [PubMed]
46. Ryabukhin, D.S.; Turdakov, A.N.; Soldatova, N.S.; Kompanets, M.O.; Ivanov, A.Y.; Boyarskaya, I.A.; Vasilyev, A.V. Reactions of 2-carbonyl- and 2-hydroxy(or methoxy)alkyl-substituted benzimidazoles with arenes in the superacid CF_3SO_3H. NMR and DFT studies of dicationic electrophilic species. *Beilstein J. Org. Chem.* **2019**, *15*, 1962–1973. [CrossRef] [PubMed]
47. Patalag, L.J.; Loch, M.; Jones, P.G.; Werz, D.B. Exploring the π-system of the (aza-)BOIMPY scaffold: Electron-rich pyrrole moieties working in concert with electron-depleted meso-positions. *J. Org. Chem.* **2019**, *84*, 7804–7814. [CrossRef] [PubMed]

48. Wang, S.; Guan, L.; Zang, J.; Xing, K.; Zhang, J.; Liu, D.; Zhao, L. Structure-based design of novel benzimidazole derivatives as Pin1 inhibitors. *Molecules* **2019**, *24*, 1198. [CrossRef]
49. Qin, H.; Miao, Y.; Xu, J.; Bi, Q.; Qu, W.; Liu, W.; Feng, F.; Sun, H. A facile and efficient [4+2] annulation reaction of sulfur ylides: Access to *N*-fused benzimidazoles. *Org. Chem. Front.* **2019**, *6*, 205–208. [CrossRef]
50. Zheng, H.-L.; Chen, X.-L.; Li, T.; Yin, Z.; Zhang, Y.; Kurmoo, M.; Zeng, M.-H. Manipulating clusters by use of competing N,O-chelating ligands: A combined crystallographic, mass spectrometric, and DFT study. *Chem. Eur. J.* **2018**, *24*, 7906–7912. [CrossRef]
51. Wang, W.; Xu, D.; Sun, Q.; Sun, W. Efficient aliphatic C-H bond oxidation catalyzed by manganese complexes with hydrogen peroxide. *Chem. Asian J.* **2018**, *13*, 2458–2464. [CrossRef]
52. Politanskaya, L.; Selivanova, G.A.; Panteleeva, E.V.; Tretyakov, E.V.; Platonov, V.E.; Nikul'Shin, P.V.; Vinogradov, A.S.; Zonov, Y.V.; Karpov, V.M.; Mezhenkova, T.V.; et al. Organofluorine chemistry: Promising growth areas and challenges. *Russ. Chem. Rev.* **2019**, *88*, 425–569. [CrossRef]
53. Makarov, A.G.; Selikhova, N.Y.; Makarov, A.Y.; Malkov, V.S.; Bagryanskaya, I.Y.; Gatilov, Y.V.; Knyazev, A.S.; Slizhov, Y.G.; Zibarev, A.V. New fluorinated 1,2-diaminoarenes, quinoxalines, 2,1,3-arenothia(selena)diazoles and related Compd. *J. Fluor. Chem.* **2014**, *165*, 123–131. [CrossRef]
54. Finger, G.C.; Reed, F.H.; Burness, D.M.; Fort, D.M.; Blough, R.R. Aromatic fluorine compounds. II. 1,2,4,5-Tetrafluorobenzene and related compounds. *J. Am. Chem. Soc.* **1951**, *73*, 145–149. [CrossRef]
55. Campbell, J.E.; Hewitt, M.C.; Jones, P.; Xie, L. Heteroaryl Compounds and Methods of Use Thereof. U.S. Patent No. WO 2011/150156 A2, 1 December 2011.
56. Allen, F.H.; Kennard, O.; Watson, D.G.; Brammer, L.; Orpen, A.G.; Taylor, R. Tables of bond lengths determined by X-ray and neutron diffraction. Part 1. Bond lengths in organic compounds. *J. Chem. Soc. Perkin Trans. II* **1987**, S1–S19. [CrossRef]
57. DcOria, E.; Novoa, J.J. On the hydrogen bond nature of the C–H···F interactions in molecular crystals. An exhaustive investigation combining a crystallographic database search and *ab initio* theoretical calculations. *Cryst. Eng. Comm.* **2008**, *10*, 423–436.
58. Rybalova, T.V.; Bagryanskaya, I.Y. C.-F . . . π, F . . . H., and F . . . F intermolecular interactions and F-aggregation: Role in crystal engineering of fluoroorganic compounds. *J. Struct. Chem.* **2009**, *50*, 741–753. [CrossRef]
59. Lannes, A.; Suffren, Y.; Tommasino, J.B.; Chiriac, R.; Toche, F.; Khrouz, L.; Molton, F.; Duboc, C.; Kieffer, I.; Hazemann, J.-L.; et al. Room temperature magnetic switchability assisted by hysteretic valence tautomerism in a layered two-dimensional manganese-radical coordination framework. *J. Am. Chem. Soc.* **2016**, *138*, 16493–16501. [CrossRef] [PubMed]
60. Prasanna, M.D.; Guru Row, T.N. C–halogen···π interactions and their influence on molecular conformation and crystal packing: A database study. *Cryst. Eng.* **2000**, *3*, 135–154. [CrossRef]
61. Lorenzo, S.; Lewis, G.R.; Dance, I. Supramolecular potentials and embraces for fluorous aromatic molecules. *New J. Chem.* **2000**, *24*, 295–304. [CrossRef]
62. Ooi, H.C.; Suschitzky, H. Practicable syntheses of 2-hydroxymethyl-substituted benzimidazoles and 2-formylbenzimidazole. *J. Chem. Soc. Perkin Trans. 1* **1982**, *12*, 2871–2875. [CrossRef]
63. Sheldrick, G.M. *SHELX-97. Programs for Crystal Structure Analysis (Release 97-2)*; University of Göttingen: Göttingen, Germany, 1998.
64. Sheldrick, G.M. Crystal structure refinement with SHELXL. *Acta Cryst. Sect. C Struct. Chem.* **2015**, *71*, 3–8. [CrossRef]
65. *SADABS, v. 2008-1*; Bruker AXS: Madison, WI, USA, 2008.
66. Spek, A.L. PLATON. In *A Multipurpose Crystallographic Tool*; Utrecht University: Utrecht, The Netherlands, 2003.
67. Spek, A. Single-crystal structure validation with the program PLATON. *J. Appl. Crystallogr.* **2003**, *36*, 7–13. [CrossRef]
68. Macrae, C.F.; Edgington, P.R.; McCabe, P.; Pidcock, E.; Shields, G.P.; Taylor, R.; Towler, M.; van de Streek, J. Mercury: Visualization and analysis of crystal structures. *J. Appl. Crystallogr.* **2006**, *39*, 453–457. [CrossRef]



© 2020 by the authors. Licensee MDPI, Basel, Switzerland. This article is an open access article distributed under the terms and conditions of the Creative Commons Attribution (CC BY) license (http://creativecommons.org/licenses/by/4.0/).